Synthesis and Properties of New Fluoroelastomer Nanocomposites from Tailored Anionic Layered Magnesium Silicates (Hectorite)

Madhuchhanda Maiti, Anil K. Bhowmick

Rubber Technology Centre, Indian Institute of Technology, Kharagpur 721302, India

Received 20 August 2007; accepted 13 August 2008
DOI 10.1002/app.29089
Published online 17 October 2008 in Wiley InterScience (www.interscience.wiley.com).

ABSTRACT: In the field of polymer clay nanocomposites, naturally occurring smectite group of clays are the most commonly used nanofillers. In the present work, smectite group clay, hectorite was synthesized in the laboratory with an intention to understand the structure–property relationship of polymer nanocomposites, with special reference to the characteristics of the nanoclays. The nanocomposites were prepared using these synthetic clays and fluoroelastomer by a solution mixing process. The clays and their nanocomposites were characterized by using X-ray diffraction, X-ray fluorescence, infra-red spectroscopy, and transmission electron microscopy. It was observed that clay formation was a function of the concentration of the constituent materials. The gallery spacings and surface areas of synthetic clays are higher than those of the natural clay. Mechanical, dynamic mechanical, swelling, and thermal properties of these nanocomposites were also studied. The properties of these nanocomposites were compared with the nanocomposites obtained from natural clays, available commercially. Synthetic clay filled samples showed better properties than the natural clay filled samples, e.g., synthetic hectorite filled sample exhibited 75% increment in tensile strength and 24% improvement in 100% modulus compared with the natural hectorite based system. The results were explained with the help of thermodynamics and morphology. © 2008 Wiley Periodicals, Inc. J Appl Polym Sci 111: 1094–1104, 2009

Key words: synthetic hectorite; nanocomposites; elastomers; fluoropolymers; clay

INTRODUCTION

The field of nanocomposite has gained considerable interest during the last two decades. Nanocomposites in the widest sense are defined as materials consisting of two or more components having at least one dimension in the nanometer range.[1] Among all the nanofillers, clay minerals are the most common ones. Polymer nanocomposites have enhanced material properties, like better mechanical properties, improved fire retardancy, thermal stability, higher stiffness and toughness, and improved gas barrier properties.[2–6] There are many reviews reporting tremendous property improvement in nanocomposites at a very low filler loading.[7–10]

But almost all reports were based on natural nanoclays. One of the major problems associated with the use of natural clays is that, although these materials may be cheap and readily available, the properties are sometimes difficult to control due to fluctuation in purity and composition obtained from various sources.[11] The gallery spacing and surface area of clays can also be controlled by synthesizing it. The change in clay structure with the variation in concentration of its constituents has been still unexplored. The synthesis of organohectorites and their nanocomposites based on polyethylene oxide (PEO) and polyvinyl alcohol (PVA) have been done by Carrado et al.[11–16] Though there are some papers on fluoroelastomers natural clay,[17,18] the effect of synthetic clay and variation of clay structure on the properties of fluoropolymer nanocomposites has not been studied so far.

In our earlier studies, we have reported the effects of natural unmodified montmorillonite as well as organoclays on the properties of general and special purpose rubbers and thermoplastic elastomers.[19–22] It is also observed that fluoroelastomer gives best properties and morphology with unmodified natural montmorillonite.[22–24] Subsequently, we synthesized montmorillonite clays and found that these clays can enhance tensile strength and modulus by 94 and 7%, respectively, compared with the natural clay.[25] Along with montmorillonite (MMT), hectorite is the most widely used nanoclay. Hectorite belongs to same smectite group as montmorillonite having T-O-T structure but of different composition and gallery gaps. Hence, in this work, the hectorite clays were prepared and characterized. The nanocomposites

Correspondence to: A. K. Bhowmick (anilkb@rtc.iitkgp.ernet.in).

TABLE I
Different Compositions for Hectorite-Like Layered Silicate Synthesis with the Elemental Analysis of Products

Sample	Starting materials	Elemental analysis, % (from SEM-EDX)	Elemental analysis, % (XRF)
NH	Natural hectorite	Na 2.35 Mg 15.95 Si 34.29 Ca 46.23 Fe 1.18	–
SH0	0.048 M $MgCl_2$, $6H_2O$ 0.01M LiF 0.022M SiO_2	Mg 30.52 Si 69.48	MgO 35.54 SiO_2 62.70
SH1	0.048M $MgCl_2$, $6H_2O$ 0.01M LiF 0.072M SiO_2	Mg 22.58 Si 77.42	MgO 25.73 SiO_2 72.49
SH2	0.048M $MgCl_2$, $6H_2O$ 0.01M LiF 0.007M SiO_2	Mg 49.95 Si 50.05	–
SH3	0.160M $MgCl_2$, $6H_2O$ 0.01M LiF 0.022M SiO_2	Mg 49.35 Si 50.65	–
SH4	0.015M $MgCl_2$, $6H_2O$ 0.01M LiF 0.022M SiO_2	Mg 22.38 Si 77.62	–

based on this synthetic hectorite were also developed and their properties were studied extensively and also compared with the natural hectorite based systems.

EXPERIMENTAL

Materials used

Viton B-50 (a terpolymer of vinylidene fluoride (VF2), hexafluoropropylene (HFP) and tetrafluoroethylene (TFE), density 1850 kg m^{-3} at 25°C, 68% F, Mooney Viscosity, ML $_{1+10}$ at 120°C = 39) was procured from DuPont Dow Elastomers, Freeport, TX. Natural hectorite was obtained from The Source Clay Repository, West Lafayette, IN. Methyl ethyl ketone was supplied by Nice Chemicals Pvt. Ltd., Cochin, India. Hexamethylene diamine carbamate (DIAK #1) was supplied by NICCO Corporation Ltd., Shyamnagar, India. Magnesium chloride-hexahydrate and lithilum fluoride were procured from LOBA Chemie Pvt. Ltd., Mumbai, India. Ammonia solution (25%) was supplied by S.D. Fine-Chem. Ltd., Mumbai, India. Silica sol (LUDOX HS-30) was obtained from Sigma-Aldrich Chemie GmbH, Steinheim, Germany.

Synthesis of hectorite-like layered silicates

In a beaker, magnesium chloride [$MgCl_2$, $6H_2O$] was dissolved in water and mixed with 32 mL of 2*N* ammonium hydroxide to crystallize fresh magnesium hydroxide [$Mg(OH)_2$]. It was then washed for several times with water. In a round-bottom flask, lithium fluoride [LiF] was dissolved in water (Table I reports the molar ratio of different starting materials). $Mg(OH)_2$ was then added to LiF solution. The resultant slurry was then stirred for about 15 min before addition of silica sol [Ludox HS-30, Na^+ stabilized, 30% water dispersion]. Different molar ratios of starting materials, used for this synthesis are reported in Table I. The pH was kept an approximately 9–10. Then, water was added to produce a approximately 2 wt % solid suspension, and was refluxed with continuous stirring for 48 h at 100°C. This process was similar to the procedure described by Carrado et al.[11] The products were isolated by centrifugation, washed, and then air dried.

Preparation of rubber-clay nanocomposites

The rubber was first dissolved in methyl ethyl ketone (20 wt % solution). The layered silicates, dispersed in methyl ethyl ketone, were added to the rubber solution and thoroughly stirred to make a homogeneous mixture, which was then kept in air at room temperature to drive off the solvents. DIAK #1 (3 phr) was then mill mixed. The samples were then cured at optimum cure time (8 min) under 5 MPa pressure and 160°C temperature in a hydraulic press.

Different compositions and their designation are registered in Table II.

X-ray diffraction studies

For the characterization of the rubber nanocomposites, X-ray diffraction studies (XRD) studies were performed using a PHILIPS X-PERT PRO diffractometer in the range of 2–40° (for powder silicate

TABLE II
Different Formulations for Fluoroelastomer-Clay Nanocomposites and Their Designation

Composition	Designation
Viton B-50 + 3 phr DIAK #1	F
Viton B-50 + 4phr NH + 3 phr DIAK #1	FNH4
Viton B-50 + 4phr SH0 + 3 phr DIAK #1	FSH0-4
Viton B-50 + 4phr SH1 + 3 phr DIAK #1	FSH1-4
Viton B-50 + 4phr SH4 + 3 phr DIAK #1	FSH4-4
Viton B-50 + 16phr NH + 3 phr DIAK #1	FNH16
Viton B-50 + 16phr SH0 + 3 phr DIAK #1	FSH0-16

samples) and 2–10° (for composites) with Cu target ($\lambda = 0.154$ nm) at a scanning rate of 0.5°/min. Then, d-spacing of the clay particles was calculated using the Bragg's law. The samples were placed vertically in front of the X-ray source. The detector was moving at an angle of 2θ, while the sample was moving at an angle of θ.

Energy-dispersive X-ray spectroscopy

Energy-dispersive X-ray spectroscopy (EDX) of the powder clay samples was performed in an Oxford EDX system attached to the Scanning Electron microscope (JEOL JSM-800).

Infra-red spectroscopy

Infra-red spectroscopy study was done in Perkin-Elmer Spectrum RX 1, in the range 400–4000 cm^{-1} by casting a very thin film of nanocomposites on potassium bromide (KBr) pellet (approximately 1% dispersion of nanocomposite in methyl ethyl ketone) at room temperature. For powder silicate samples, the study was performed making a pressed pellet with KBr. An average of 32 scans was reported here.

Transmission electron microscopy

The powder clay samples were dispersed in acetone using ultrasonication. Two drops of the dispersed sample was placed over carbon coated copper grid.

The samples for TEM analysis of the nanocomposites were prepared by ultra cryomicrotomy. Freshly sharpened glass knives with cutting edge of 45° were used to get the cryosections of 100 nm thickness. Since these samples were elastomeric in nature, the sample temperature during ultra cryomicrotomy was kept constant at –60°C (which was well below glass transition temperature, [T_g]), at which the samples existed in hard glassy state, thus facilitating ultra cryomicrotomy. The cryosections were collected and directly supported on a copper grid of 200-mesh size. The microscopy was performed using JEOL-2010 electron microscope with LaB_6 filament, operating at an accelerating voltage of 200 KV. The images were analyzed with "UTHSCSA-Image Tool" software.

BET surface area

Surface area measurement by BET N_2 adsorption method was done using QUANTACHROME (NOVA 1200) machine.

X-ray fluorescence spectroscopy

X-ray fluorescence spectroscopy (XRF) was performed in PHILIPS – PW 2404 X-ray spectrometer. The samples were prepared by fusing the layered silicates with lithium tetraborate at 1200°C. Only a few representative samples were analyzed for comparison with SEM-EDX data.

Mechanical properties

Tensile specimens were punched out from the molded sheets using ASTM Die-C. The tests were carried out as per the ASTM D 412-98 method in a Universal Testing Machine (Zwick 1445) at a cross-head speed of 500 mm/min at 25°C. The average of three tests is reported here.

Dynamic mechanical thermal analysis

The dynamic mechanical spectra of the nanocomposites were obtained by using a dynamic mechanical thermal analysis (DMTA) IV, (Rheometric Scientific, New Jersey, USA) dynamic mechanical thermal analyzer. The sample specimens (height 15 mm, width 10 mm, thickness 1 mm) were analyzed in tensile mode at a constant frequency of 1 Hz, a strain of 0.01% and a temperature range from –50 to 80°C at a heating rate of 2°C/min. Storage modulus (E′), loss modulus (E″), and loss tangent (tan delta) were measured as a function of temperature for all the samples under identical conditions. The temperature corresponding to the peak in tan delta versus temperature plot was taken as the glass-rubber transition temperature (T_g).

Swelling studies

Sorption experiments were performed by placing the previously weighed test samples into the respective liquid containers (gram of sample vs. volume of liquid 1 : 100) maintained at 30°C temperature in an oven (S.C. Dey & Co., Kolkata, India). MEK was used as the solvent. At periodic intervals, the test samples were removed from the liquid containers and the extra solvent on the surface was wiped out quickly with blotting paper and the samples were

weighed immediately. After weighing, the samples were placed back into the original test bottles.

Thermal analysis

Thermogravimetric analysis (TGA) and differential thermogravimetric (DTG) were done using a Perkin–Elmer Pyris Diamond TG/DTA machine in air at a heating rate of 10°C /min. The temperature range was 50–700°C.

RESULTS AND DISCUSSION

Characterization of different layered silicates

The initial information obtained on every new synthetic sample is XRD pattern. XRD provides a look into the extent of clay crystallization and its layered nature. Figure 1 includes XRD patterns of natural and synthetic hectorites for comparison purposes. Only SH0, SH1, and SH4 samples show a characteristic (001) reflection for smectite group clays within 2–10° region. This region has been reported to indicate gallery heights in clay structure.[26]

In the case of SH0, the peaks at 5.5° (d-spacing, d = 1.6 nm), 19.5° (d = 0.48 nm), and 34.9° (d = 0.25 nm) correspond to (001), (110,020), and (130) hectorite reflections, respectively.[11] For SH1 sample, the peaks are at 5.8° (d = 1.5 nm), 19.5 and 34.9°. For SH4 sample, these peaks are at 6.2° (d = 1.4 nm), 19.7, and 34.9°. The results indicate that with changing ratio of the starting materials the d-spacing of (001) plane shifts slightly. In this context, it is worth mentioning that Carrado et al. found d-spacings of 1.95–2.08 nm when the clay minerals were hydrothermally crystallized with direct incorporation of a series of water soluble PVA of different molecular weight.[13]

For natural hectorite, NH, the d(001) is 1.3 nm. Hence, it can be concluded that with changing ratio of constituent materials, the d(001) spacing can be increased without any incorporation of organic moiety, as usually done for organophilic clays. Hence, for a polar rubber like fluoroelastomer, where unmodified natural clays exhibit better results,[22] this method of increasing d-spacing would be beneficial. The natural hectorite shown in Figure 1 demonstrates peaks similar to those observed for the synthetic minerals. But the natural hectorite, even after extensive cleaning, still contains $CaCO_3$, quartz, and (Mg, Fe, Ca)SiO_3 impurities [as indicated from several peaks present at 23, 26.5, 29.5, 30.8, 31.5, 35.9, and 39.5°].[11] Also, the results obtained from SEM-EDX studies show that there is fair amount (approximately 46%) of calcium present in the sample (Table I).

The only crystalline product among the starting materials is a layered $Mg(OH)_2$. The XRD pattern of this is clearly distinct from that of the clay. There is no

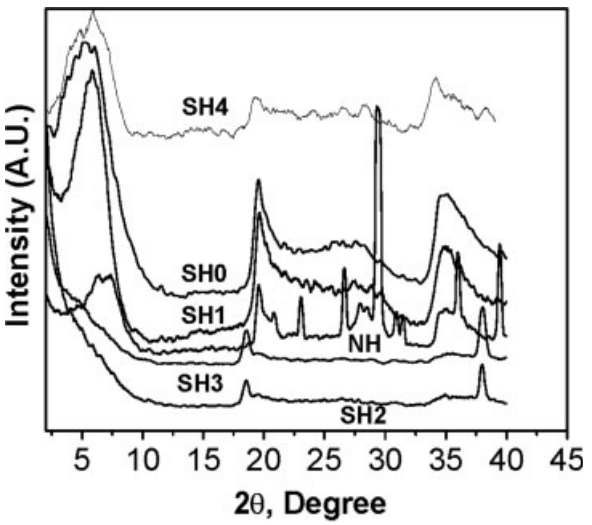

Figure 1 XRD of different synthetic hectorite–clay-like layered silicates.

sign of $Mg(OH)_2$ in SH0, SH1, and SH4, which would display peaks at 18.5° (d = 0.48 nm) and 38° (d = 0.24 nm) for the (001) and (101) reflections, respectively. Interestingly, at the same reaction condition, layered silicates can not be obtained for SH2 and SH3 samples, where the ratio of starting materials was different. For both the samples, there are two peaks at 18.5 and 38° indicating presence of unreacted $Mg(OH)_2$.

It is interesting to see that every composition does not yield layered clays. It can be seen from Table I that only when the ratio of magnesium to silica is 1 : 1.8–1 : 3.4, the layered silicates were formed. The range has been specified from both SEM-EDX and XRF studies. The clay materials are mainly composed of magnesium, silica, and water, with alkalies and sometimes alkaline earth metals.[26] There are several concepts about how these chemical constituents are combined to give clay materials. It may be possible that the elements are present as amorphous mixtures without any definite composition or structure. Then layered clay may not be formed. As the theories say that the mineral kaolinite is the essential constituent of all clay materials and in our case elements not fitting into the composition of it did not form clay.[26] Another case may be that the particle size of the constituents was not fine enough (i.e., < 1 μm) and hence there was no clay formation. The initial ingredients may lack zeolite like minerals, which are the necessary constituents of clay materials according to another clay formation theory.[26] But still there is no definite theory which can specify the driving forces responsible for clay material formation from the chemical constituents.[26]

Figure 2 illustrates the TEM of SH0. The particles are mainly in the form of aggregates of layered particles with individual thickness in the nanometer range (3–5 nm). Particles are having length of $\sim$ 50–200 nm.

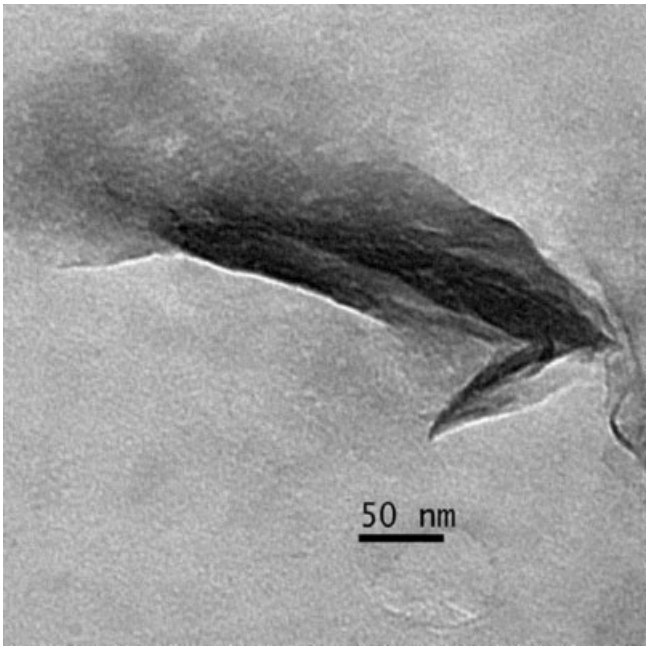

Figure 2 TEM image of SH0.

Figure 3 shows the Infra-red spectroscopy (IR) spectra of different synthetic hectorites along with natural one. In the studies of clay minerals, the peaks due to structural OH and Si—O groups play an important role in the differentiation of clay minerals from each other.[27] The IR spectra can show the difference in stacking the sheets as well as in the occupancy of the octahedral and tetrahedral sites. Mainly two regions show characteristics of clays: (1) the —OH stretching region in between 3400 and 3700 cm^{-1} and (2) the region below 1200 cm^{-1}. The —OH stretching band varies with the nature of the octahedral atom to which the —OH group is attached. The hectorite, where —OH is attached to Mg, shows a single stretching band $\sim$ 3680 cm^{-1},[27] which is also evident in the case of SH0, SH1, and SH4. But the samples SH2 and SH3 show two bands in that region. This may be also indicating that hectorite type clay has not been formed in these two cases.

TABLE III
Particle Size, Basal Spacing and BET Surface Area of Natural and Synthetic Layered Silicates

Sample	Particle size (nm)	Basal spacings (nm)	BET N_2 surface area (m^2/g)
NH	30.2	1.30	71.0
SH0	13.7	1.60	176.1
SH1	14.4	1.50	159.4
SH4	20.2	1.40	–

In the 1300–400 cm^{-1} region, the spectra of clay show Si—O stretching, bending and —OH bending. Figure 3 shows only one broad complex stretching band $\sim$ 1012 cm^{-1} for Si—O stretching, characteristic of hectorites. This peak is present in each and every sample. The —OH attached to Mg in hectorite gives bending vibration at 655 cm^{-1}, which is visible in the case of NH, SH0, SH1, and SH4. In every sample, there is a peak at around 1640 cm^{-1}, probably for —Mg—O. In the natural hectorite, there is another prominent peak at 1432 cm^{-1}. This may be for the impurities like quartz.[28]

Particle size of different clays was calculated from the X-ray diffractograms according to Warren[29]:

$$\text{Particle size} = \frac{1.84\lambda}{B\cos\theta} \quad (1)$$

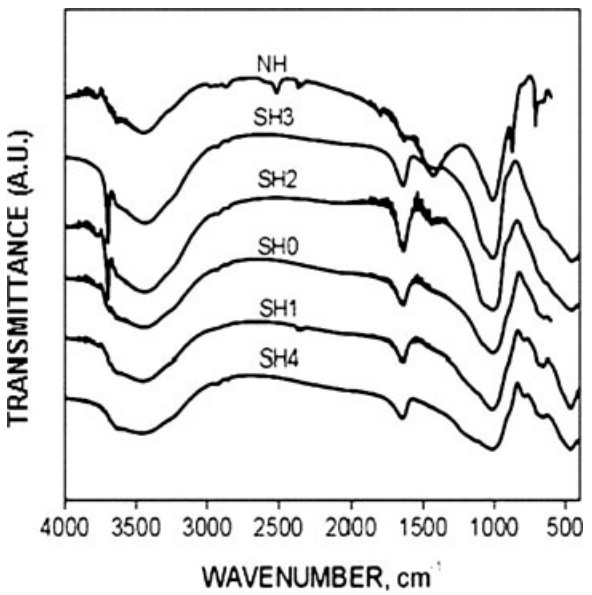

Figure 3 IR spectra of different hectorites.

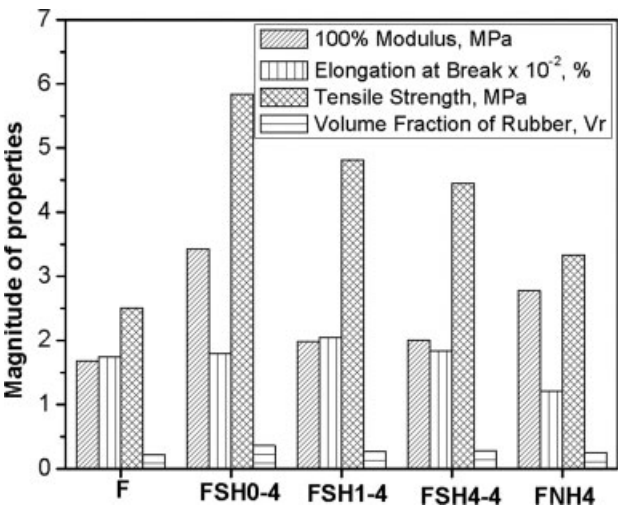

Figure 4 Comparison of physicomechanical properties of different hectorite-like layered silicate-based nanocomposites.

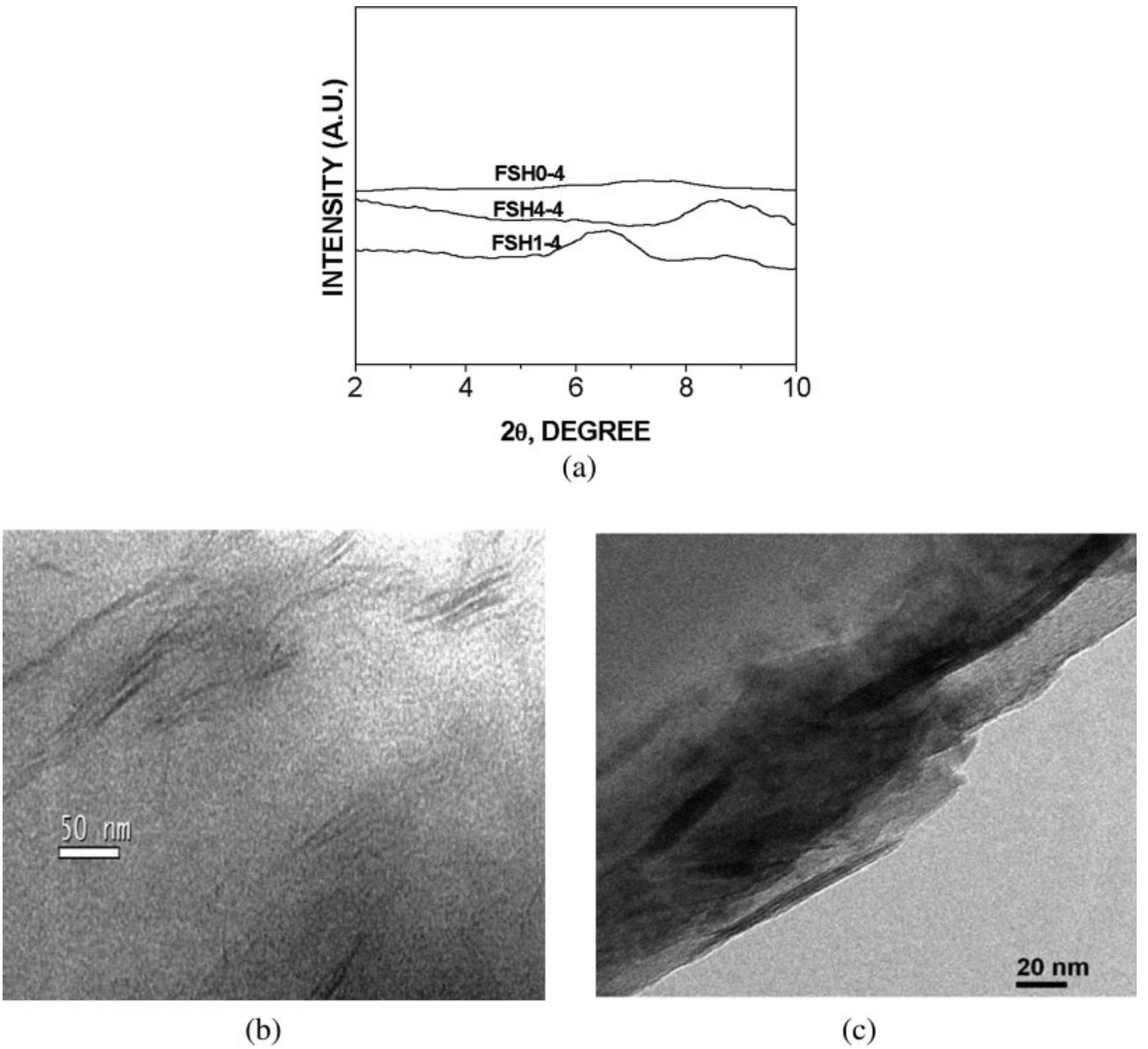

Figure 5 (a) XRD of different hectorite-like layered silicate based nanocomposites (at 4 phr loading) (b) TEM of FSH0-4 (c) TEM of FSH1-4.

where λ = incident wavelength of CuK_α radiation, B = width of (110) peak at half maximum in radians.

The particle sizes are reported in Table III. The synthetic clays show smaller particle size than that of the natural hectorite. SH0 is having smallest particle size followed by SH1 and SH4. Hydrothermally synthesized hectorites have lower particle size than the natural one. It is worth mentioning here, that the particle size calculated from eq. (1) should not be taken as a quantitative one but it can provide a qualitative comparison between various clays. This equation is being used to determine the size of a two-dimensional layer in the plane of the layer from two-dimensional reflection.[29] The BET surface area of synthetic hectorite clays are around 2.5 times more than that of the natural clay.[11]

Nanocomposites with hectorites

Figure 4 shows a comparison of mechanical properties of different hectorite-like layered silicates based composites at 4 phr loading. As we did not get layered products in the case of SH2 and SH3, we eliminated these two systems.

Compared with natural hectorite, all the synthetic materials impart better properties. Natural hectorite based sample shows 33% improvement in tensile strength over the control fluoroelastomer. Among the synthetic samples, FSH0-4 exhibits the best result followed by FSH1-4 and FSH4-4. FSH0-4 registers 134% increment in tensile strength and 104% improvement in 100% modulus over the control system. This particular sample exhibits 75% increment

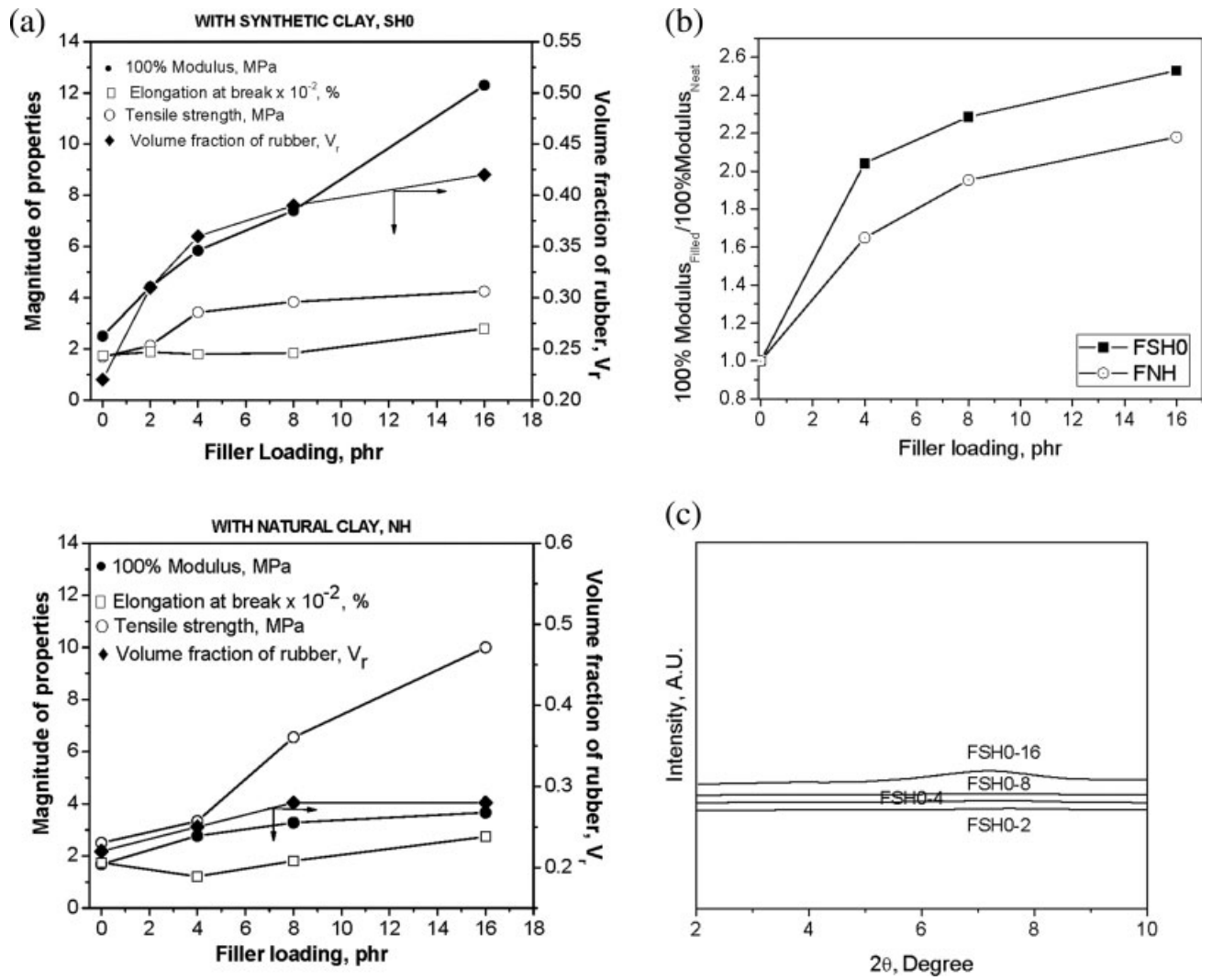

Figure 6 (a) Physicomechanical properties of different nanocomposites with varying filler loading (b) Plot of $\frac{100\%\text{Modulus}_{\text{Filled}}}{100\%\text{Modulus}_{\text{Neat}}}$ with varying filler loading (c) XRD of SH0 based nanocomposites (with varying filler loading) (d) TEM of FSH0-16 (e) XRD of natural hectorite clay-based nanocomposites (with varying filler loading) (f) TEM of FNH16.

in tensile strength and 24% improvement in 100% modulus compared with the natural hectorite based system. The variation in strength with changing clay type may be explained with the different characteristic of clays. The synthetic clays give better result compared with the natural one, as the synthetic clays are much purer than the natural counterpart. Moreover, the XRD studies of the clays reveal that the d-spacing of the synthetic clays is higher than the natural one (Table III). Lower particle size and higher surface area enhance the polymer–filler interaction in the case of synthetic clays. Now, among different synthetic clays, SH0 is having highest d-spacing. Hence, in this case, the interaction between polymer and clay will be facilitated leading to better improvement in properties. This is further evidenced from the XRD of different nanocomposites shown in Figure 5(a). There is no peak in the case of FSH0-4, while there are humps at 6.5 and 8.6° for FSH1-4 and FSH4-4, respectively. It indicates that there are some ordering present in these samples, rendering lower mechanical properties. TEM images also support the XRD study. The TEM micrographs of FSH0-4 and FSH1-4 are shown in Figure 5(b–c). The image shows that the clay particles are homogeneously distributed with a single platelet thickness of ~ 1 nm in FSH0-4. The length of the particles lies in between 50 and 80 nm. The better polymer filler interaction might have broken the clay layers. The image of FSH1-4 shows intercalated structure.

Effect of filler loading on mechanical properties is illustrated in Figure 6(a). With increasing filler loading both tensile properties and modulus increase in the case of natural as well as synthetic hectorite. We studied SH0 based nanocomposites, as it showed the best properties among all the synthetic hectorites. At every filler loading, synthetic clay based nanocomposites exhibit better result compared with the

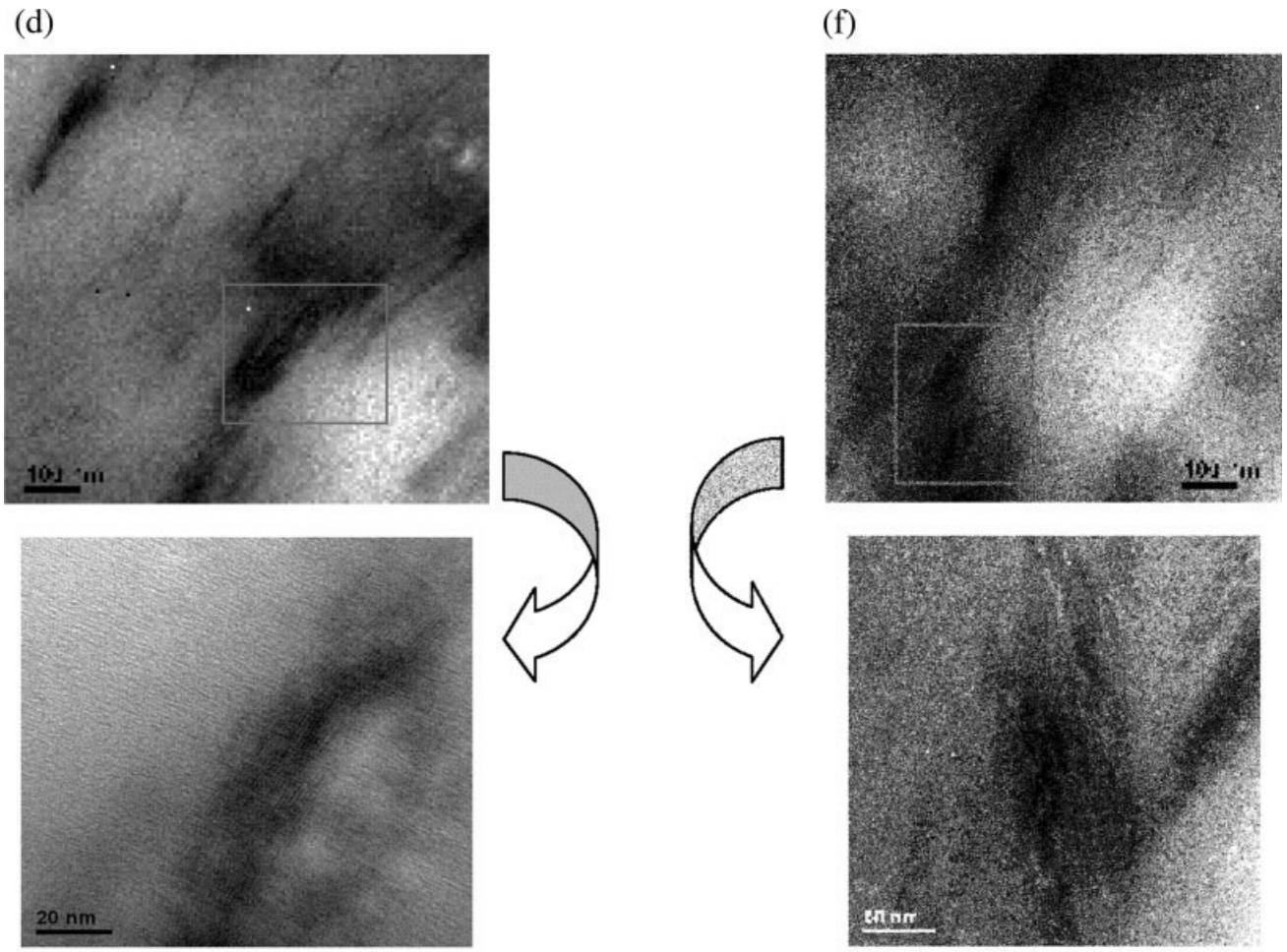

Figure 6 *(Continued from previous page)*

natural one. The plot of $\frac{100\%\text{Modulus}_{\text{Filled}}}{100\%\text{Modulus}_{\text{Neat}}}$ for both the clays at different loadings is shown in Figure 6(b). $\frac{100\%\text{Modulus}_{\text{Filled}}}{100\%\text{Modulus}_{\text{Neat}}}$ of synthetic clay filled samples is found to be 1.2 times of natural-clay filled samples at every loading. It is also interesting to note that in the case of synthetic clay, till 16 phr loading, the clay does not agglomerate, as evident from XRD [Fig. 6(c)] and TEM [Fig. 6(d)]. But natural clays start agglomerating at 8 phr loading as evident from XRD [shown in Fig. 6(e)]. The TEM micrograph of FSH0-16 shows that the clay particles are well dispersed in the matrix. From a large scan it seems that there are some intercalations along with exfoliation, though

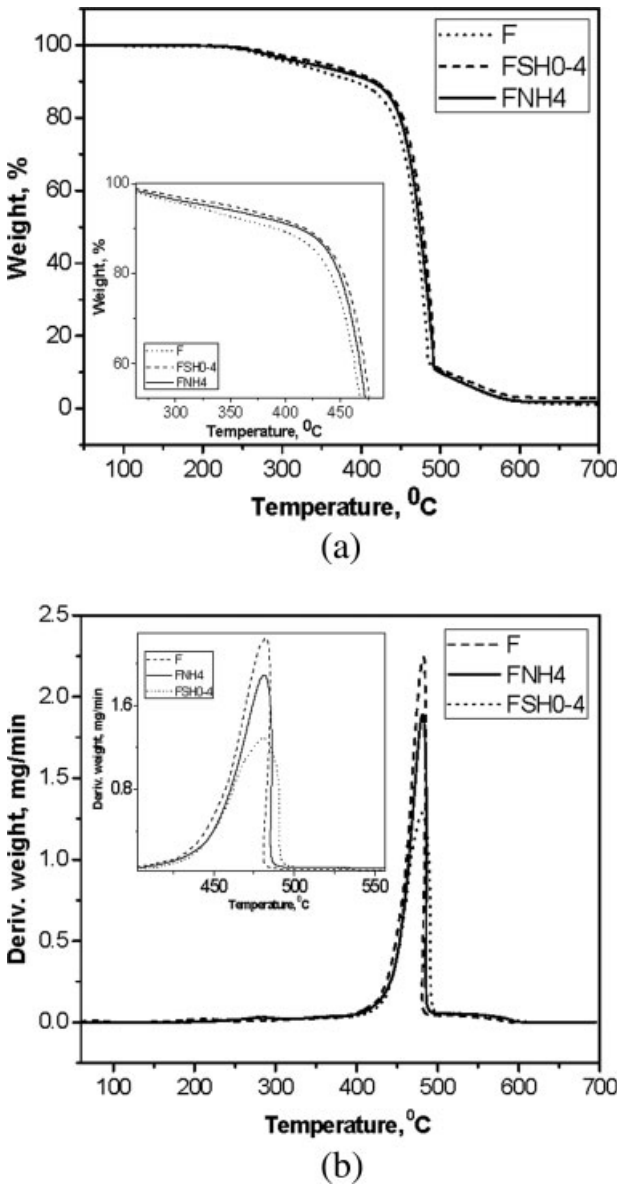

Figure 7 Typical (a) TG (b) DTG curves of F, FNH4, and FSH0-4.

the XRD does not reveal it. XRD sometimes is unable to give the information about intercalation if the layers are well separated.[2,9] The close view of the intercalated portion shows that the clay layers are $\sim$ 1 nm in thickness, but they are present in an ordered arrangement. The distance between two platelets is $\sim$ 2 nm. Lengthwise these particles are broken down, having $\sim$ 50 nm length. The TEM micrograph of FNH-16 [Fig. 6(f)] shows that the clay particles are not so well dispersed in the matrix. Also, the small size scan reveals the agglomeration of clay in the matrix. The thickness of the clay layers are $\sim$ 10 nm.

Typical TG curves and the corresponding derivative thermogravimetric (DTG) curves obtained at a heating rate of 10°C/min for F, FNH4-4 and FSH0 are shown in Figure 7(a,b). These TG curves correspond to a single-stage degradation with well defined initial and final degradation temperatures and might have been a result of a random chain scission process. T_{onset} and T_{max} values for F, FNH4 and FSH0-4 are 458, 459, 464°C and 481, 481, and 483°C, respectively. T_{max} was determined from the respective DTG curve peaks. Decomposition rate was 2.23, 1.89, 1.27 mg/min. for F, FNH4 and FSH0-4, respectively. Hence, thermal stability is also enhanced with the addition of synthetic hectorites compared with the natural clay based nanocomposite and the control.

Swelling studies also support the above results, as the volume fraction of rubber in the swollen gel is highest for FSH0-4 (Fig. 4). A sorption-plot (i.e., mass uptake vs. square root of time, $t^{1/2}$) at 30°C is given in Figure 8. All the curves show initially a linear increase, and later tend to level off. The plateau regions of these curves give the maximum sorption values, M_∞, which is lowest in the case of FSH0-4. The diffusion coefficients, calculated following our earlier communication,[24] of F, FSH0-4 and FNH4 are 1.43×10^{-8}, 0.26×10^{-8}, and 0.60×10^{-8} cm^2 s^{-1}, respectively. Hence, FSH0-4 exhibits lowest diffusion coefficient also. This may be due to the fact that SH0 is more interactive with the rubber due to larger gallery spacing and smaller particle size. Because of these, FSH0-4 is more resistant to solvent than the other nanocomposites. With increasing filler loading, volume fraction of rubber steadily increases in the case of synthetic hectorite, though it remains almost same for the natural hectorite [graph shown in Fig. 6(a)]. In the case of natural clay, it starts to agglomerate at higher loading and the interaction between

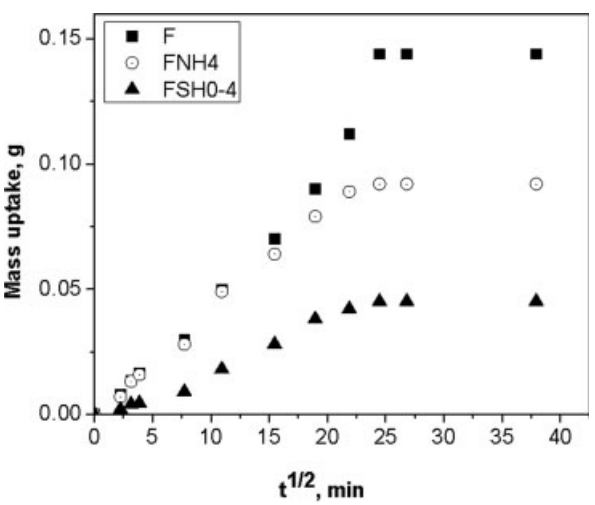

Figure 8 Sorption curves for different nanocomposites at 30°C (solvent MEK).

TABLE IV
Dynamic Mechanical Properties of Hectorite-Like Layered Silicate Based Nanocomposites

Sample name	T_g (°C)	Tan δ_{max} at T_g	Log E′ at 25°C (Pa)	Log E′ at 60°C (Pa)
F	−23	1.23	6.14	6.09
FSH0-2	−9	1.19	6.19	6.12
FSH0-4	−8	1.19	6.35	6.25
FSH0-8	−8	1.14	6.62	6.60
FSH0-16	−8	0.97	6.85	6.73
FNH-16	−21	1.16	6.35	6.34
FSH1-4	−18	1.16	6.20	6.15
FSH4-4	−19	1.15	6.18	6.12

clay and polymer reduces. As a consequence solvent resistance also reduces.

Same behavior has been observed in the case of dynamic mechanical properties also. The dynamic mechanical properties are reported in Table IV. The storage modulus in the rubbery plateau region increases with the addition of filler (Fig. 9). At 4 phr loading, the modulus is highest for FSH0-4 compared with the other two synthetic clay based nanocomposites. The tan delta peak shifts towards higher temperature with the addition of the filler (Fig. 9). Though the change is marginal for natural hectorite based system, there is remarkable change in the synthetic clay based samples. There is around 15°C temperature shift in FSH0-4 compared with the control.

The storage modulus increases gradually with the increasing loading of synthetic clay [Fig. 9(a)]. But for these composites, the tan delta peak is more or less at same position [Fig. 9(b)]. The tan δ_{max} decreases with increasing filler loading indicating better polymer–filler interaction. The reduction is most in the case of FSH0-16. The decrease of tan δ_{max} is the result of a reduction of the relative quantity of bulk rubber "active" in the dynamic transition. As filler fraction is more at 16 phr loading, also the fillers are mostly exfoliated with some intercalations; more number of the rubber-chains can interact with the filler, reducing the active free-chain numbers. Hence, lowering of tan δ_{max} is much pronounced in FSH0-16.

Explanations in terms of thermodynamics

From the results discussed so far, it can be summarized that the synthetic clays provide better mechanical, swelling, thermal and dynamic mechanical properties compared with their natural counterparts. Among all synthetic hectorites, FSH0-4 gives best overall properties. It can also be observed from the XRD and TEM studies that this system is exfoliated compared with the other nanocomposite systems. Also, the lower particle size, higher surface area and larger gallery gaps of SH0 make it exhibit better polymer–filler interaction compared with other synthetic as well as natural clays of their same group.

The better polymer–filler interaction and the favoring of nanocomposite formation can be predicted from the thermodynamic point of view.[22] The free energy change of the system after mixing the clay in fluoroelastomers may be given as follows:

$$\Delta G_E = \Delta H_E - T\Delta S_E, \quad \text{for elastomers} \tag{2}$$

$$\Delta G_C = \Delta H_C - T\Delta S_C, \quad \text{for clays} \tag{3}$$

Therefore, total free energy change of the system is

$$\Delta G_S = \Delta H_S - T\Delta S_S = \Delta H_S - T(\Delta S_E + \Delta S_C) \tag{4}$$

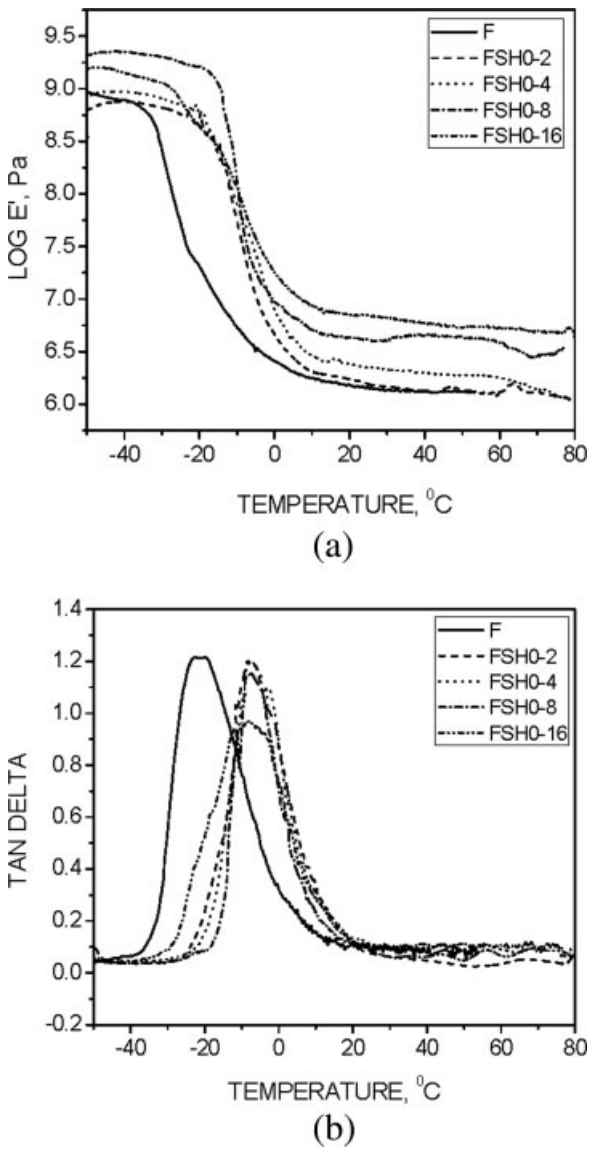

Figure 9 (a) LOG E′ vs. temperature plot of SH0 based nanocomposites (b) Tan δ vs. temperature plot of SH0 based nanocomposites.

TABLE V
Change in Enthalpy

Sample name	Peak position (cm^{-1})	ΔH (kcal/mol)
F	1197	–
FNH4	1195	−0.47
FSH0-4	1180	−4.01
FSH1-4	1188	−2.12
FSH4-4	1190	−1.65

From the expression, ΔG_S value will be negative and hence the most favorable interaction between the clay and the rubber will take place when ΔH_S is negative and ΔS_S is positive.

When polymer chains enter into the gallery of the clay, they reside in a restrained form, i.e., ΔS_E is negative. In contrast, the expansion of the gallery by elastomer chains causes the entropy change in the clay, ΔS_C to be positive. If the clays are exfoliated, this may probably compensate the entropy loss associated with the confinement of elastomer chains.

Hence, ΔG_S is mostly dependent on ΔH_S value. ΔH_S has been calculated for different systems from the IR spectra (not shown here) using Fowkes's equation,[30]

$$\Delta H = 0.236 \times \Delta v \quad (5)$$

The values are reported in Table V. ΔH_S is negative for all the systems.

In the case of hectorite-like clays, it is most negative in the case of FSH0-4, followed by FSH1-4, FSH4-4 and FNH4. As a result, the mixing of the synthetic clay with the fluoroelastomer is more favorable than that of the natural one. This fact is reflected in all the properties.

CONCLUSIONS

Different hectorite type layered clays have been synthesized in the laboratory. The synthetic materials were characterized using XRD, SEM-EDX, XRF, BET surface area measurement, IR, and TEM.

At the same reaction condition, clay formation depends on the concentration of its constituents. All the compositions do not yield a layered silicate.

Synthetic clays show larger d-spacing than the natural one. The synthetic clays are also much purer than the natural one.

The fluoroelastomer based nanocomposites were prepared using these different synthetic clays and characterized by using XRD and TEM.

Better mechanical, dynamic mechanical, swelling and thermal resistance properties were observed with the synthetic clays compared with its natural counterpart. SH0 based nanocomposite shows best properties among all the hectorite-type clays.

Synthetic clay based nanocomposites are thermodynamically more favorable than the natural clay filled ones.

The properties can be explained with the help of morphology and thermodynamics.

References

1. Lan, T.; Kaviratna, P. D.; Pinnavaia, T. J Chem Mater 1995, 7, 2144.
2. Maiti, M.; Sadhu, S.; Bhowmick, A. K. J Polym Sci Part B: Polym Phys 2004, 42, 4489.
3. Jang, B. N.; Costache, M.; Wilkie, C. A. Polymer 2005, 46, 10678.
4. Giannelis, E. P. Adv Mater 1996, 8, 29.
5. Yano, K.; Usuki, A.; Okada, A. J Polym Sci Part A: Polym Chem 1997, 31, 2289.
6. Xu, B.; Zheng, Q.; Song, Y.; Shangguan, Y. Polymer 2006, 47, 2904.
7. Sinha Ray, S.; Okamoto, M. Prog Polym Sci 2003, 28, 1539.
8. LeBaron, P. C.; Wang, Z.; Pinnavaia, T. J Appl Clay Sci 1999, 15, 11.
9. Alexandre, M.; Dubois, P. Mater Sci and Eng 2000, 28, 1.
10. Okamoto, M. Rapra Review Report 2003, 14, Report 163.
11. Carrado, K. A. Appl Clay Sci 2000, 17, 1.
12. Carrado, K. A.; Thiyagarajan, P.; Song, K. Clay Miner, 1997, 32, 29.
13. Carrado, K. A.; Thiyagarajan, P.; Elder, D. L. Clays Clay Miner 1996, 44, 506.
14. Sandı, G.; Carrado, K. A.; Joachin, H.; Lu, W.; Prakash, J. J Power Sources 2003, 492, 119.
15. Carrado, K. A.; Sandi, G.; Kizile, R.; Seifert, S.; Castagnola, N. App Clay Sci 2005, 30, 94.
16. Sandi, G.; Kizilel, R.; Carrado, K. A.; Fernández-Saavedra R.; Castagnola N. Electrochim Acta 2005, 50, 3891.
17. Kader, M. A.; Lyu, M.; Nah, C. Compos Sci Technol 2006, 66, 1431.
18. Kader, A. M.; Nah, C. Polymer 2004, 45, 2237.
19. Sadhu, S.; Bhowmick, A. K. Rubber Chem Technol 2003, 76, 0860.
20. Maiti, M.; Sadhu, S.; Bhowmick, A. K. J Appl Polym Sci 2006, 101, 603.
21. Maiti, M.; Bandyopadhyay, A.; Bhowmick, A. K. J Appl Polym Sci 2006, 99, 1645.
22. Maiti, M.; Bhowmick, A. K. J Polym Sci Part B: Polym Phys 2006, 44, 162.
23. Maiti, M.; Bhowmick, A. K. Polymer 2006, 47, 6156.
24. Maiti, M.; Bhowmick, A. K. J Appl Polym Sci 2007, 105, 435.
25. Maiti, M.; Bhowmick, A. K. Compos Sci Technol 2008, 68, 1.
26. Grim, R. Applied Clay Mineralogy; Mcgraw Hill: New York, 1962.
27. Madejova, J. Vib Spectrosc 2003, 31, 1.
28. Available at: http://webbook.nist.gov/, accessed on 26 June 2006.
29. Warren, B. E. Phys Rev 1941, 59, 693.
30. Fowkes, F. M.; Tischler, D. O.; Wolfe, J. A.; Lannigan, L. A.; Ademu-John, C. M.; Halliwell, M. J. J Polym Sci: Part A: Polym Chem 1984, 22, 547.